THE JOURNAL OF PHYSICAL CHEMISTRY C

ARTICLE

pubs.acs.org/JPCC

Production of Palladium Nanoparticles by Pulsed Laser Ablation in Water and Their Characterization

G. Cristoforetti,*[,†] E. Pitzalis,[‡] R. Spiniello,[‡] R. Ishak,[§] and M. Muniz-Miranda[∥]

[†]National Institute of Optics, Research Area of National Research Council, Via G. Moruzzi 1 - 56124 Pisa, Italy

[‡]Institute of Chemistry of Organometallic Compounds, Research Area of National Research Council, Via G. Moruzzi 1 - 56124 Pisa, Italy

[§]Department of Chemical Engineering and Material Science, University of Pisa, Via Diotisalvi 2 - 56126 Pisa, Italy

[∥]Department of Chemistry, University of Florence, Via della Lastruccia 3 - 50019 Sesto Fiorentino, Italy

ABSTRACT: Nanosized particles of pure palladium were produced by pulsed laser ablation in aqueous solution, with and without the addition of sodium dodecyl sulfate as the surfactant agent. The work was motivated by the strong catalytic effect of Pd particles in many chemical reactions. The influence of experimental parameters, such as laser energy and beam focusing as well as surfactant concentration, on the laser ablation process, nanoparticle mass yield, and nanoparticle properties was investigated via plasma imaging, UV−visible spectroscopy, transmission electron microscopy/energy dispersive spectroscopy (TEM-EDS) analysis, and measurement of ζ potential. The surface-enhanced Raman scattering activity of nanoparticles was used for the monitoring of their adsorption capability on the metal surface during catalysis processes.

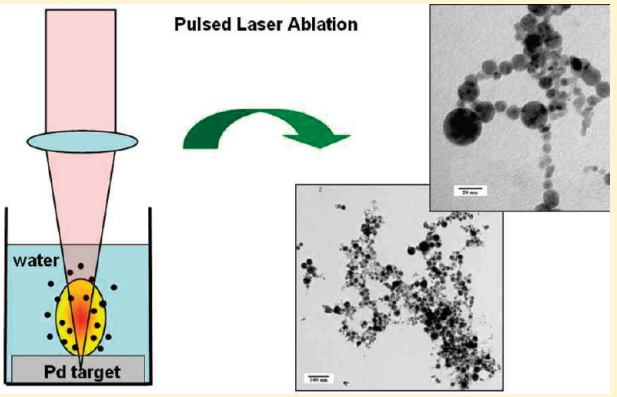

INTRODUCTION

The interest in nanosized particles (NPs) has hugely grown because of their peculiar physical and chemical properties related to quantum size effects with respect to bulk samples and to the enhancement of surface properties due to the large surface/volume ratio. In the past decade, a large part of the scientific effort was focused on the setup of techniques and methodologies of NP synthesis that allow adequate control of particles size distribution, shape, and crystallinity, adequate temporal stability, and, at the same, a production rate sufficiently high for real applications and industrial scale-up. In recent years, Pulsed Laser Ablation in Liquid (PLAL) was introduced as a production technique and tested for different composition NPs, including metals, semiconductors, carbon-based nanomaterials and alloys. In the PLAL technique, a laser pulse is focused on a target immersed in a solvent generating a microplasma that rapidly expands, quenches, and decays in times on the order of microsecond. During such a process, the atomized material removed from the target, interacting with the species originated from the solvent, nucleates and begins to grow up to the formation of NPs. Several advantages of PLAL technique with respect to the most used chemical methods can be mentioned, e.g., the possibility, in principle, of utilizing the technique for producing NPs of whatever composition, the possibility of controlling NP properties (size, shape, and crystallinity) by tuning several experimental parameters (laser energy and wavelength, solvent composition, surfactant, etc.), and finally the production of pure colloids free of chemical agents such chemical precursors or reducing agents and, in particular cases, free of chemical stabilizers. The last point appears to be determinant for the application of NPs in biomedical or biological applications, where chemical agents can be harmful and reduce cell viability after NP treatment; moreover, the absence of ligands on the particle surface enhances the possibility of their functionalization with biomolecules, making them very effective as biomarkers or for targeted cell therapies.[1,2] Furthermore, the bare surface of NPs is very attractive for all the applications exploiting their chemical properties, as for example catalysis purposes. This encouraged many research groups to focus their attention on the PLAL synthesis of those NPs that are more promising for catalytic applications such as Ni, Pd, and Pt, investigating the influence of experimental parameters (including the concentration of surfactant) on the NP properties and their catalytic effect for specific reactions. Mafunè et al.[3] investigated the effect of laser energy and of sodium dodecyl sulfate (SDS) concentration on the size distribution and the stability of Pt NPs produced by PLAL in water. The authors showed that the most stable NPs were obtained at a 0.01 M SDS concentration but a considerable stability was also obtained for bare (no surfactant) Pt NPs, with a half-life period longer than 500 days and a slight tendency to coalesce. The stability of surfactant-free platinum

Special Issue: Laser Ablation and Nanoparticle Generation in Liquids

Received: September 28, 2010
Revised: November 23, 2010
Published: December 20, 2010

NPs was explained by the adsorption of OH^- on their surface, which produces an electrostatic repulsive force impeding their coalescence. Park et al.[4] investigated the catalytic activity during an electron-transfer reaction between $Fe(CN)_6^{3-}$ and $S_2O_3^{2-}$ of Pt NPs produced by PLAL in water and successively stabilized with different typical stabilizing polymers, such as poly(vinyl pyrrolidone), poly(vinyl sulfate), and polyethyleneimine.

Kim et al.[5] showed that Ni NPs produced by PLAL in pure water exhibited a catalytic activity (yield ~20%) for the preparation of 3-arylpropanenitrile from benzylchloride and bromoacetonitrile under the mild condition without any activation, whereas the laser ablated Ni NPs stabilized with SDS (10^{-2} M) as well as the commercial Ni particles larger than submicrometer size did not show such activity. According to the authors, the low yield obtained could be due to partial oxidation of Ni NPs in solution.

Palladium has peculiar properties as a catalyst, finding several applications in organic synthesis as well as in the reduction of environmental pollutants.[6,7] It is also widely employed in hydrogen storage[8] and very recently in biomedical research.[9−12] All these applications need the use of palladium in a finely divided state, like in the case of colloidal NPs, which can adsorb great amounts of ligand due to their large surface area.

Hwang et al.[13] investigated the catalytic activity of suspended nanosized palladium NPs produced by PLAL in ethyl acetate solution, with and without the addition of tetraoctylammonium bromide (TC_8ABr) as stabilizer, toward various olefin hydrogenation reactions. Both TC_8ABr−Pd and bare-Pd NPs were proven to be more powerful olefin hydrogenation catalysts with respect to the commercially available 10% Pd/C; however, the catalytic activity of Pd NPs stabilized with TC_8ABr, despite the partial capping of Pd surface, was higher than that of bare-Pd NPs, because of their significantly smaller dimensions resulting in an estimated fraction of surface atoms going from 40% to 7.5% from TC_8AB-Pd to bare Pd NPs. This last result evidences that the catalytic activity of a NP system is not exclusively affected by the percentage of bare surface of the particle but by many other parameters, including the total surface area, the aggregation and coalescence degree, the size distribution, the surface structure, the shape of the NPs, and finally by the presence of a support. For this reason, besides optimizing the production of catalytic NPs and probing their catalytic activity toward different reactions, it is necessary to perform a careful characterization of the NPs produced in order to correlate effectiveness in catalysis with NP properties.

In this work, palladium NPs were produced by pulsed laser ablation (PLA) in aqueous solution, with and without SDS, and successively characterized in view of their application as catalysts to be performed in a subsequent step. The attention of this work is then focused on the understanding and optimization of the production process, by varying several experimental parameters (laser energy, SDS concentration, lens focus position), and the physical-chemical characterization of the NP ensembles, through several analytical and spectroscopic techniques, including ultraviolet−visible (UV−vis) spectroscopy and transmission electron microscopy (TEM) measurements accompanied with energy dispersive spectroscopy (EDS). For these NPs it is also necessary to verify the capability of adsorbing organic ligands, in view of possible functionalizations. Surface-enhanced Raman scattering (SERS) spectroscopy[14] allows obtaining useful information about the adsorption of molecules on nanostructured metal surfaces, because it combines the molecular recognition provided by the vibrational spectroscopy with an extremely high sensitivity due to the giant enhancement of the adsorbate Raman signal, usually up to 10^6−10^7 factors. This is mainly important for monitoring catalytic processes of reactive or intermediate species occurring at the Pd surface. Hence, SERS measurements have also been performed by adsorption of organic ligand onto Pd particles obtained by laser ablation.

EXPERIMENTAL METHODS

Laser ablation was performed by focusing a Nd:YAG laser pulse (λ = 1064 nm, τ = 12 ns), perpendicularly aligned to the target surface and operating at a repetition rate of 10 Hz, by means of a lens of 25 cm focal length. The target, a pure palladium plate with purity of >99.9%, was fixed at the bottom of a glass vessel filled with 8 mL (height above the target = 4 mm) of aqueous solution of SDS. Ultrapure (u.p.) water prepared with a purification system (Purelab Pro, USF) was used in all the operations. SDS was purchased from Sigma Aldrich (ReagentPlus ≥98.5%).

Each stage of NP production lasted for 20 min. The glass vessel was rotated and translated during the ablation process in order to prevent effects due to crater formation.

Several experimental parameters were varied, including the laser energy (range 3−158 mJ), the lens-to-sample distance (17 < LTSD < 25 cm) and the concentration of SDS (from 0 to 10^{-2} M). The variation of the first two parameters allows an independent adjustment of both the laser energy and the laser spot onto the target surface. Tuning of these two parameters resulted in a range of laser fluences spanning in the range 1.6−2000 J cm^{-2} (irradiance in the range 1.3×10^8 to 1.7×10^{11} W cm^{-2}).

The as-produced colloids were analyzed by UV−vis spectroscopy on a Perkin-Elmer Lambda 25 UV−vis spectrometer, using quartz cells (Hellma) with 1 cm light path. UV−vis spectra were measured immediately after the generation process and successively at time intervals of 2−3 days up to a time of 30 days after the production stage to evaluate the stability of the NPs over time.

Particle size and distribution have been investigated using TEM-EDS analysis performed on a Philips CM12 microscope working at 120 kV equipped with Bruker Quantax EDX analysis. A semiquantitative analysis has been also done to verify the chemical composition of the NPs. A few drops of the supernatant colloid solution were placed on a carbon coated copper grid and allowed to dry at a temperature around 80 °C.

TEM images were analyzed using a semiautomatic plug-in of the ImageJ software to determine the NPs size distribution. A quantity of at least 800−1200 NPs was measured for each sample.

The crystalline structure of the NPs was verified using the selected area electron diffraction (SAED) technique in TEM and high-resolution TEM.

ζ potential values were obtained with a 90 plus Analyzer (Brookhaven Instruments Co., NY, USA) from dynamic light scattering measurements at a temperature of 25 °C by means of the Smoluchowski equation.

The SERS spectra in Pd colloids were recorded using the 514.5 nm line of a Coherent Argon ion laser (power: 50 mW), a Jobin-Yvon HG2S monochromator equipped with a cooled RCA-C31034A photomultiplier and a data acquisition facility.

Power density measurements were performed with a power meter instrument (model 362; Scientech, Boulder, CO, USA) giving ~5% accuracy in the 300−1000 nm spectral range.

The SERS spectra for Pd particles deposited on glass were measured using a Renishaw RM2000 microRaman apparatus, coupled with a diode laser source emitting at 785 nm. Sample irradiation was accomplished using the ×100 microscope objective of a Leica Microscope DMLM. The beam power was ~3 mW, the laser spot diameter was adjusted between 1 and 3 μm. Raman scattering was filtered by a double holographic Notch filters system and collected by an air-cooled CCD detector. The acquisition time for each measurement was 10 s. All spectra were calibrated with respect to a silicon wafer at 520 cm^{-1}.

RESULTS AND DISCUSSION

During the irradiation of the target, the color of the solution changes to yellow in the case of low ablation rate and to brown in the case of strong NP production.

(a). Laser Ablation Process. The variation of LTSD and of laser energy affects the ablation rate and therefore the net NP production rate because (a) it produces a variation of the laser fluence and of the ablation spot dimensions, and (b) it can induce a plasma at the water−air interface or inside the water, which partially or totally absorbs the pulse energy via inverse bremsstrahlung processes. The latter effect is clearly seen in Figure 1a−c, where time-integrated images of the plasma induced by one single pulse are shown.

While at low fluences, the laser pulse completely reaches the target surface inducing the main plasma (Figure 1a), a secondary weak plasma at the air−water interface appears already at a fluence of ~12 J cm^{-2}, corresponding to an irradiance of ~1 GW cm^{-2} (Figure 1b), after ~1 min of laser ablation. The secondary plasma becomes stronger with increasing laser fluence (Figure 1c) and progressively absorbs a larger portion of laser energy; at the opposite, the plasma on the target surface becomes progressively weaker. It is important to remark that the appearance of the secondary plasma occurs at a fluence level much lower than that corresponding to the breakdown threshold of water, which is ~600 J cm^{-2} (threshold irradiance ~50 GW cm^{-2}; see ref 15). Moreover, we noted that the plasma at the air−water interface became stronger as the time elapses, suggesting that plasma formation is facilitated by the formation of NPs in the solution, which noticeably lowers the breakdown threshold during the first minutes of PLA. The occurrence of a plasma at the air−water interface at irradiance values lower than the water breakdown threshold was already observed in previous works,[15,16] showing that the absorption of laser pulse via inverse bremsstrahlung or photoionization processes (depending on laser wavelength) results in a progressive reduction of the energy and of the duration of the pulse reaching the target surface. In particular, the ignition threshold found in the present work (~1 GW cm^{-2}) is very similar to the value 2.0 ± 0.5 GW cm^{-2} found by Berthe at al.,[16] who used a 25 ns λ = 1064 nm laser pulse. From a practical point of view, the onset of plasma ignition at the air−water interface also corresponds to the beginning of the splashing of the liquid surface, resulting in a net loss of part of the colloid in the surrounding environment; such loss evidently becomes more severe as laser fluence increases.

In order to estimate the effects of laser fluence and of the secondary plasma on the mass removal from the target and on the formation of NPs, UV−vis spectroscopy of the colloids obtained at different irradiance levels was performed. Typical absorption spectra of Pd colloids, obtained in different experimental conditions, are reported in Figure 2. In all the cases, except at very high laser fluences, the spectra exhibit a very large band extending into the UV, which is typical of an interband transition of a metallic system, showing a quite evident peak located around 220 nm. Such spectra are qualitatively in good agreement with previous Pd experimental spectra[17,18] (where, however, a shift of the peak position due to the different composition of the solution is present), and in optimum agreement with theoretical spectra calculated by means of the Mie theory.[19]

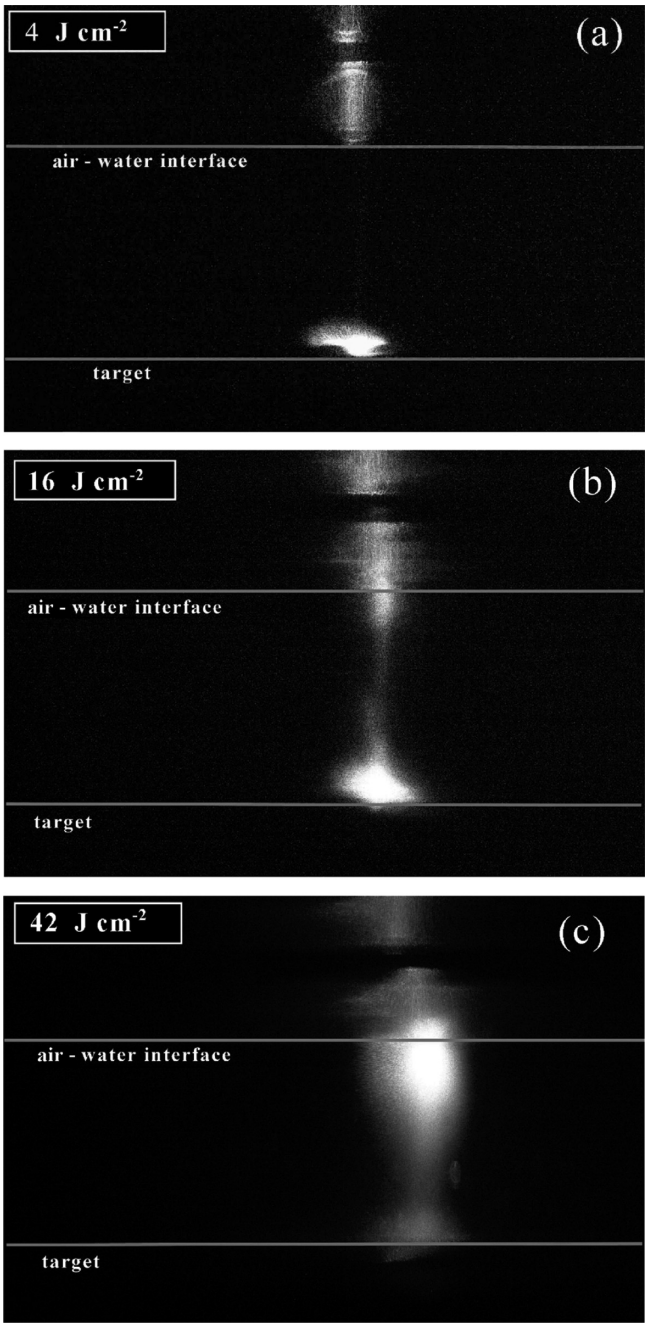

Figure 1. Time-integrated image of one-pulse laser ablation performed at different laser fluences. (a) 4 J cm^{-2}; (b) 16 J cm^{-2}; (c) 42 J cm^{-2}. The light visible above the air−water interface is spurious and due to the light scattering.

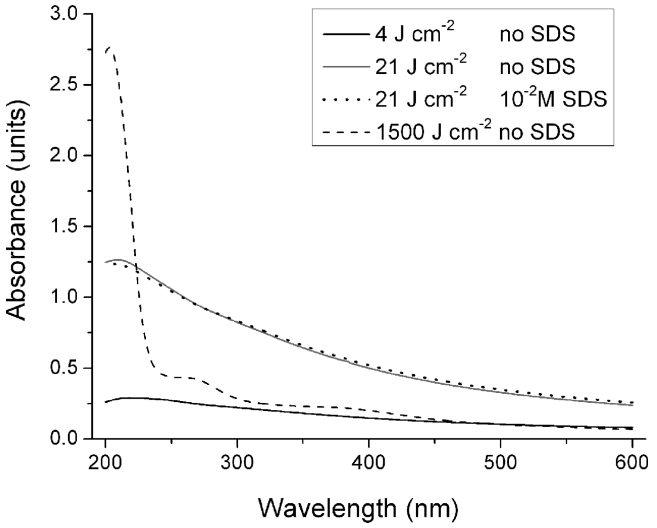

Figure 2. Absorption spectra of Pd colloids prepared under different experimental conditions.

It is significant to note that the absorption spectra obtained with and without the addition of SDS are identical (Figure 2). Finally, it is evident that the spectrum obtained at large fluence is very different, showing a high peak at ∼203 nm and two smaller peaks at ∼265 nm and ∼380 nm; at the same time, despite the high peak at ∼203 nm, the absorbance all over the spectrum is noticeably lower than that of the spectra obtained at lower fluences. The peak located at ∼203 nm is due to the absorption of ionic Pd^{2+} present in solution and begins to be clearly visible in the range of fluences between 50 and 100 J cm^{-2}, which corresponds to a situation where a strong plasma is produced at the air−water interface, and the larger part of laser energy is absorbed by it. The other two peaks at ∼265 nm and ∼380 nm, not clearly identified, could be due to the formation of other oxidized Pd species[20] or to the presence of agglomeration.

As usual,[21,22] a qualitative estimation of the total mass of NPs dispersed in the solution is obtained by the analysis of absorption spectra. In fact, according to the Mie theory and assuming the quasi-static approximation, which is valid for particles much smaller than the probing wavelength (it will be verified by the successive TEM analyses), the main contribution of the absorbance is the dipolar absorption, which is proportional to the total volume of the particles.[23] The validity of the above assumption is strengthened by the observation that the colloids prepared with and without SDS, which presumably have been produced with the same ablation rate but are characterized by different size distributions (see successive paragraph), show identical absorption spectra within experimental errors. In particular, for the mass estimation, the absorption at 320 nm was selected, which is well inside the interband transition but is far from the bands due to ionic palladium or aggregation.

The estimated total mass of NPs (in arbitrary units), produced in different experimental conditions, is reported in Figure 3a; the value represents the mass actually produced, corrected for the percentage of colloid lost for the splashing of the solution. In Figure 3b, the ablation yield per unit of surface irradiated is reported, which brings interesting information on the laser ablation process. The uncertainty of the data plotted in Figure 3a,b was estimated by the reproducibility of the measurements, which is large at low fluences (relative standard deviation

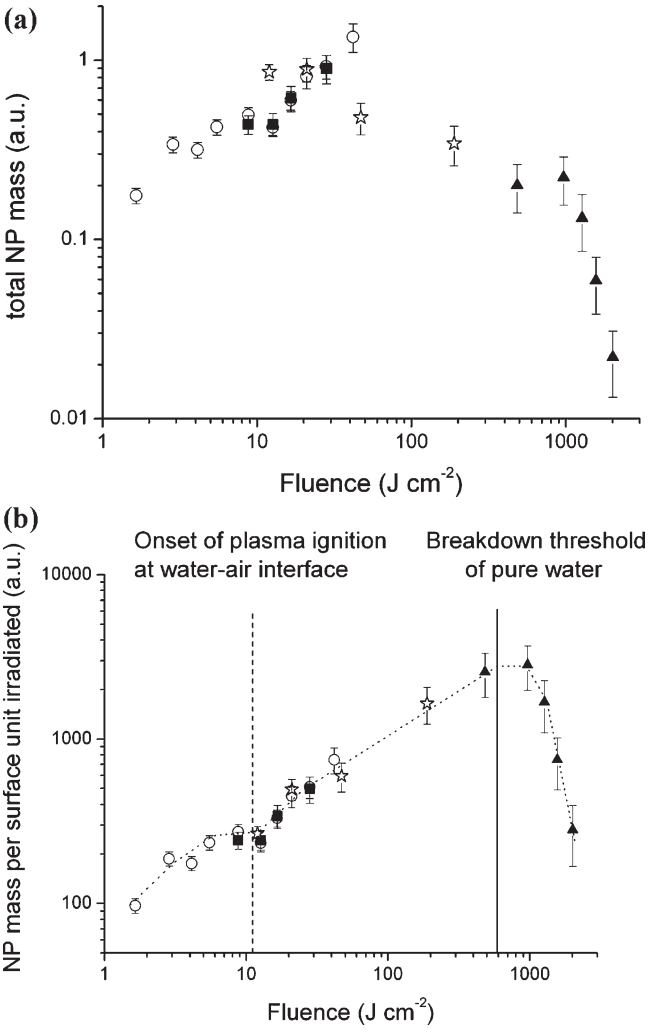

Figure 3. Trends of ablation yield and of ablation yield per surface unit irradiated, estimated by the absorption spectra analysis, as a function of laser fluence. The marks represent different experimental conditions. Circles: LTSD = 19 cm, laser energy variable, no SDS; squares: LTSD = 19 cm, laser energy variable, 0.01 M SDS; stars: LTSD variable, laser energy = 38 mJ, 0.01 M SDS; triangles LTSD = 25 cm, laser energy variable, no SDS. The error bars represent the reproducibility of the data, as reported in the text.

(RSD) = 10%), where it is affected mainly by the fluctuations of laser energy, but decreases at larger fluences (up to RSD = 50%), wherein plasma shielding and water splashing significantly affects NP production.

As evident in both of the plots, the onset of secondary plasma produces a shoulder in the NP production rate versus laser fluence plot, due to both the reduction of the energy arriving at the Pd surface and the formation of liquid splashing of the colloid. At laser fluences larger than 12 J cm^{-2}, the total NPs yield continues to grow up to values of 30−40 J cm^{-2}, when the splashing becomes severe and the NP mass begins to decrease (Figure 3a).

According to Figure 3a, the best condition for NP production rate, balancing high fluence and spot dimensions, was LTSD = 19 cm and pulse energy =38 mJ (fluence 21 J cm^{-2}). The large defocusing of the laser is selected with the aim of enlarging the ablation spot, compensating the relatively small laser fluence used for reducing liquid splashing.

The NP production rate was then measured in this condition by weighing the target before and after the production stage and by direct measurements of NP mass via atomic absorption spectroscopy (AAS), obtaining the values of ∼1.3 mg/h and ∼1.1 mg/h, respectively, which are consistent considering the experimental errors.

By observing the plot of NP mass yield per unit of ablated surface, it is evident that it continues to increase with laser fluence, despite the strong water−plasma absorption, up to the threshold of water breakdown (∼5×10^{10} W cm^{-2}, corresponding to 600 J cm^{-2}). However, such fluences are obtained by a tight laser focusing, resulting in a lower net NP production because of the small area ablated. The large values shown at high fluences can be explained by different mechanisms, which can also mutually concur to produce the effect observed. First, the water surface is not flat but bent with ripples, so that it can acts as a lens, focusing the laser beam, in a nonreproducible way shot by shot, and on larger ablation regions. Second, self-focusing due to plasma effects can also play a role in changing the index of refraction of the plasma. Finally, a different mechanism of mass removal from the surface can be hypothesized, such as reactive plasma etching of the target, as reported by Nichols et al.[24] In this case, the removal of surface atoms of the target can be caused by the interaction with the hot water−plasma, or with the shock-wave expanding in water or, finally, by the collisional sputtering produced by high-kinetic-energy ions reaching the surface. The mechanism is mainly hydrodynamic rather than thermal and can be very disruptive and visible on the target surface, considering that water plasma can absorb over 90% of the laser energy and that most of it is converted into mechanical energy;[25] it is thus clear, which is in accordance to analogous phenomena observed in ambient gas,[26] that such regime is expected to also produce melt displacement and splashing on the target surface. Very few experimental works investigated the NP production in this fluence regime, probably because of the low production rate obtained, and very little information about such a mechanism and the characteristics of NPs produced is available.

(b). Characterization of NPs . *Morphology and Size Distribution.* All the observations were made one day after the production stage, when an evident dark deposit of material was already present on the bottom of the vial where NPs were contained.

TEM micrographs of several sets of NPs, produced at different experimental conditions, are shown in Figure 4. In Figure 5, the corresponding histograms of particle size distribution are reported. At all the experimental conditions, the produced NPs are spheroidal in shape, in particular the larger ones, as clearly evident from TEM micrographs at higher magnifications, as, for example, in Figure 4d. Those produced in pure water are partially aggregated, in particular those obtained at low fluences, where a partial coalescence of particles seems also to exist. This phenomenon makes the detection of small particles (<4 nm) rather difficult and can result in a selective underestimation of small particles in the size distributions shown in Figure 5. The NPs produced in aqueous solution of SDS are clearly less aggregated than those produced in pure water, and most of the particles are clearly detached.

The size distribution of NPs in pure water markedly depends on laser energy, where the average size value increases with fluence, according to other works dealing with NP formation by PLAL.[27,28] The colloids produced at small laser fluences (Figure 5a) exhibit a narrow distribution peaked at ∼5 nm, but the real value could be slightly shifted toward smaller sizes because of possible underestimation of the smallest particles. Such desirable distribution, where large particles are rare is, however, associated with a quite small production rate, which was estimated to be ∼0.4 mg/h.

Similar narrow distributions peaked at values around 5 nm can also be obtained by using larger laser fluences with the addition of SDS to the solution (Figure 5c), with the advantage of enhancing the NPs production rate to values larger than 1 mg/h.

According to Granqvist and Buhrman,[29] if NPs are formed by nucleation and successive growth via liquid-like coalescence, the logarithms of particles volumes should have a Gaussian distribution, so that particle sizes are log-normal distributed. On the other hand, if the particle growth occurs via absorption of atomic vapor by the nuclei, the log-normal function can be unsuitable for fitting the NP size distribution because of the importance of diffusion effects during particle growth.

As shown in Figure 5, the obtained size distributions were poorly fitted by using a single log-normal function, because of an excess of large NPs. The presence of such large NPs is, however, strongly affected by the laser energy, being almost negligible at low fluence values, and by the presence of surfactant agents (Figure 5c).

Similar distributions were previously found by Nichols et al.[21] for platinum NPs and by Kabashin and Meunier[30] for gold NPs, who hypothesized a bimodal distribution associated with different mechanisms of particle formation. Also in our case, such hypothesis would be corroborated by the good fitting of the size distributions obtained by utilizing two log-normal functions, as shown in Figure 5. However, the size distributions obtained here (as well as those obtained in previous works) do not clearly show the presence of two peaks, so that the real presence of a bimodal distribution is questionable and will be discussed in the following, together with its possible reasons.

Several explanations have been given in the literature for the presence of a bimodal distribution of NPs. They rely on the concomitance or competition of different mechanisms of particles formation, which can be due to different mechanisms of mass removal from the target (vaporization, melt splashing, phase explosion, plasma etching), to different mechanisms of NP growth into the vapor, or finally to the occurrence of NPs fragmentation because of their interaction with the laser beam. Nichols et al.,[21] comparing NP size distributions with the microscope analysis of the craters in the target, suggested that the small and large distributions could be related to different mechanisms of mass removal, in particular vaporization and phase explosion. According to their results, the position of the two distributions do not change with laser fluence, but their relative contribution varies, so that the small-particles one prevails at small fluences, associated with vaporization, and the large-particles one prevails at large fluences, associated with spinodal explosion of the target. Also Kabashin and Meunier,[30] relying on TEM images and craters observation, suggested that the two distributions are associated with different mechanisms of mass removal, where the small-size particles are produced by thermal-free femtosecond ablation, and the larger ones are produced by the melt effects caused by plasma−target interaction, or plasma etching.

Also in our case, plasma etching is expected to occur and become dominant at very large fluences, where plasma breakdown is very likely to occur directly in water; on the other hand, it is very improbable that phase explosion of the target surface would occur at such large irradiances where plasma absorption is dominant, impeding the largest part of laser pulse energy to reach

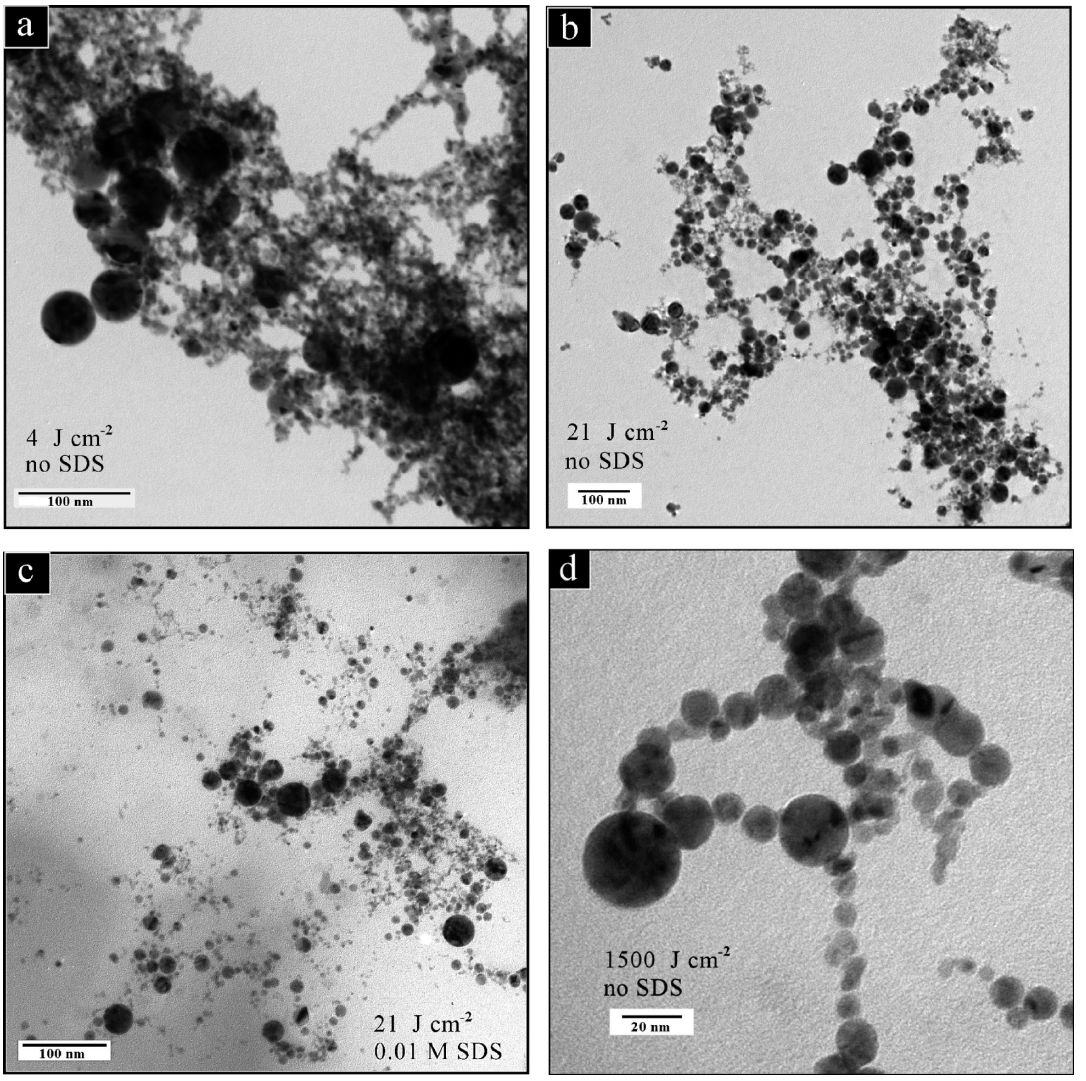

Figure 4. TEM images of Pd NPs colloids obtained under different conditions: (a) fluence = 4 J cm^{-2}, pure water; (b) fluence = 21 J cm^{-2}, pure water; (c) fluence = 21 J cm^{-2}, aqueous solution of SDS 0.01 M; (d) fluence = 1500 J cm^{-2}, pure water.

the target. In our case, nonetheless, the picture in which the two size distributions are associated with vaporization and plasma-etching, although it agrees with the progressive importance of a large component with increasing laser irradiance, collides with the near disappearance of it when surfactant agents are used. Evidently, surfactant agents affect the mechanisms of particle growth but not those of laser ablation.

Another explanation of bimodal size distribution was given by Bozon-Verduraz et al.[31] and Simakin et al.,[32] who hypothesized that smaller NPs are generated by the fragmentation of larger ones due to interaction with the laser beam. In this case, the absorption of laser radiation induces the melting of NPs, which successively split because of hydrodynamic instabilities. Such a model, however, does not explain the influence of surfactant agents on the distribution as observed in our data.

The failure of these mechanisms to explain our results cast doubts on the real presence of a bimodal distribution; at the same time, the effect of surfactant concentration on the amount of large size NPs suggests that the shape of the size distributions is related to the growth mechanism of NPs, rather than to the mechanisms of laser ablation or to photofragmentation.

A two-step NP formation mechanism can be considered for the understanding of the experimental data where a rapid phase of embryonic particle formation in the hot plume is followed by a second phase where the NPs grow via liquid-like coalescence or via absorption of atomic vapor; while the first mechanism stops a few tens of nanoseconds after laser ablation, the atoms absorption, according to Mafunè et al.,[33] ends when the atoms in the liquid environment have been mostly consumed or when the NPs have been coated by surfactant molecules. Mafunè et al.[28] showed that, in absence of surfactant agents, the growth of NPs continues for several hours after the laser ablation time. The picture agrees with the rise of the average size in the distribution as laser fluences increases, since larger pulse energies produce larger pressures in the plume and in the cavitation bubble, larger amounts of metallic atomized material and plume dimensions, and longer plume lifetimes.[34]

In the case of small laser fluence, the atomized material in the solution is limited, so that the growth via atom absorption rapidly ends because of the low collisional rates. Moreover, in that case, the decay time of temperature is smaller, so that the condensation of the plume stops earlier. In the case of high laser fluence, the decay time of plume temperature is larger, in particular in the

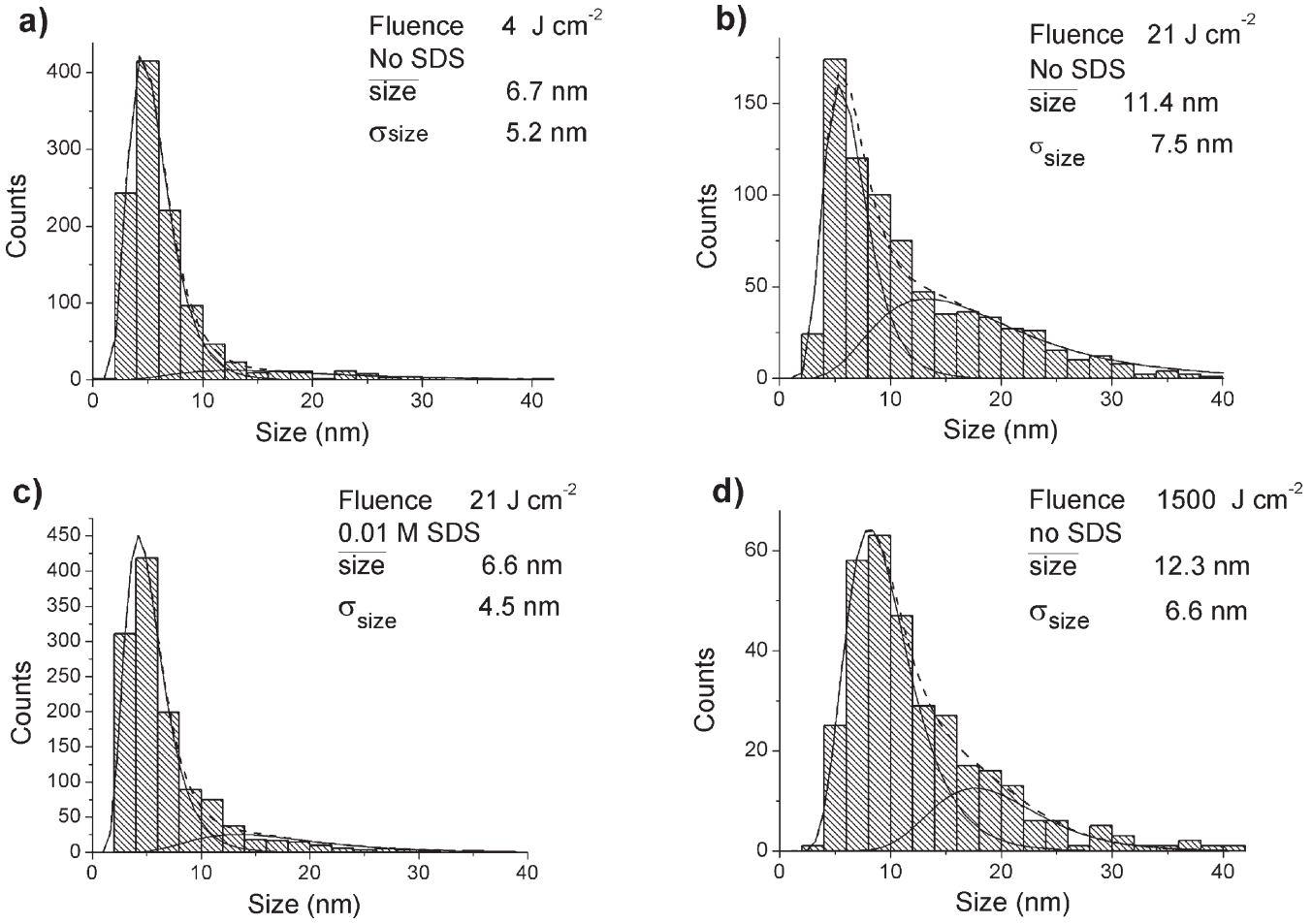

Figure 5. Size distributions of Pd NPs obtained under different conditions: (a) fluence = 4 J cm^{-2}, pure water; (b) fluence = 21 J cm^{-2}, pure water; (c) fluence = 21 J cm^{-2}, aqueous solution of SDS 0.01 M; (d) fluence = 1500 J cm^{-2}, pure water.

core, so that larger NPs are formed.[34] Moreover, the atom absorption lasts for a longer time, where ions dispersed in the solution can aggregate also to NPs or nucleation seeds produced in previous laser shots. This latter mechanism, strongly affected by diffusion, can not be adequately described by a log-normal function, as outlined by Granqvist and Burham, and produces an excess of large-particles in the size distribution. Moreover, it is evident that the production of large particles, obtained by a long-time growth in the solution, is strongly affected by the presence of surfactant agents as experimentally found.

Another complication of predicting the size distribution of NPs, which can result in a deviation from a log-normal function, is inherent to the spatial inhomogeneity of the plume and to the different cooling times of its different regions, leading to the formation of smaller NPs at the plume−liquid interface and of larger ones in the core of the plume and near the target surface, as shown by Wen et al. for PLA in a gas environment.[34]

The above model of NP formation, in conclusion, agrees with the effect of SDS in reducing the amount of large NPs and suggests that significant deviations from a single log-normal distribution can be obtained, without invoking two separate mechanisms of NP formation (which would justify a bimodal fitting).

Crystalline Structure. EDX analysis in TEM on single NPs is shown in Figure 6. The two main palladium peaks were present at 2.838 keV (Lα) and 2.990 keV (Lβ1).

The crystalline structure of the NPs is confirmed by the SAED of the NPs presented in Figure 7 revealing diffraction rings typical of a polycrystalline structure. The rings correspond to *d*-spacing of 2.24, 1.94, 1.37, 1.17 Å, respectively. These value correspond to the (111), (200), (220), and (311) planes of the face-centered cubic (f.c.c.) structure of Pd metal, respectively. Further evidence of the crystalline nature of the NPs was obtained from the HRTEM studies on the produced NPs present in Figure 8. The well-defined lattice fringes of the precipitate confirms the crystalline nature of the NPs.

Stability of the NPs. The stability of NPs produced in pure water and in 0.01 M SDS was probed. To this purpose the UV−vis absorption spectra of the colloids in a period range of 30 days were acquired. At all fluences used, except at very high values (>200 J cm^{-2}), the absorption at 320 nm of colloids in pure water decays about 7% in the first 20 days and then tends to stabilize. The addition of SDS does not seem to enhance the stability; on the contrary, the decay of absorption after 30 days increases to 15%. At large fluences, near the water breakdown threshold, at the opposite, NPs are unstable, where the absorption spectrum of the colloid decays from 40% up to ∼90% after a few days.

A confirmation of these results was given by the measurement of the ζ potential, which is a measure of the electrostatic repulsive interaction between particles dispersed in a liquid and represents an excellent indicator of the colloidal stability. ζ potential is a

dx.doi.org/10.1021/jp109281q |*J. Phys. Chem. C* 2011, 115, 5073–5083

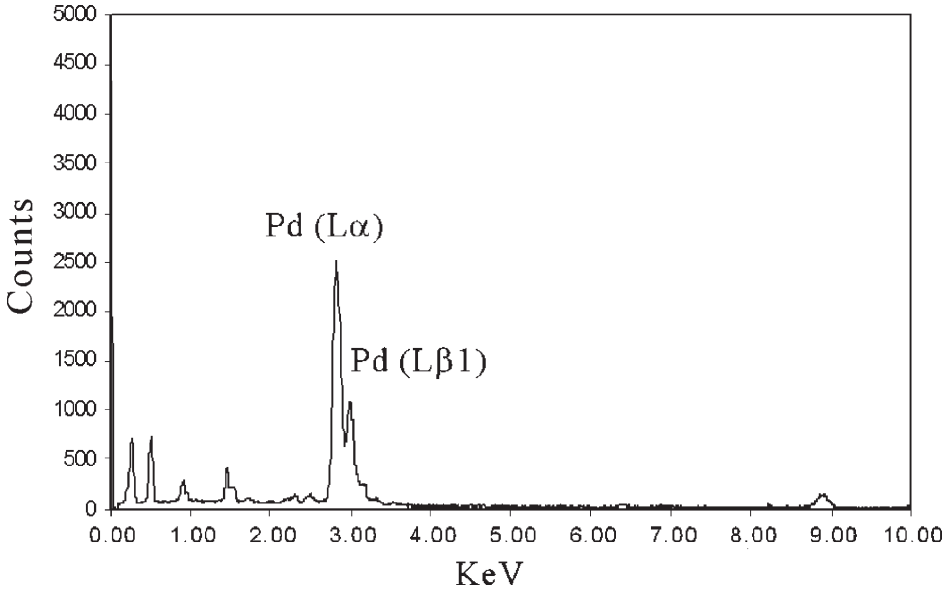

Figure 6. EDX spectrum of the NPs under TEM.

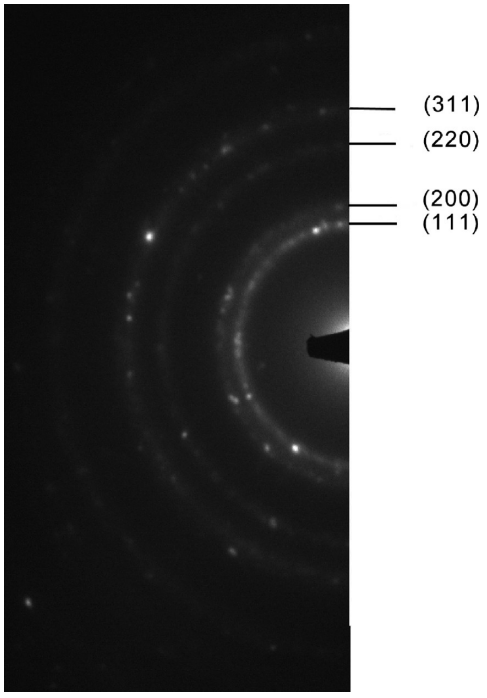

Figure 7. SAED pattern of the NPs under TEM showing the diffraction rings from Pd particles.

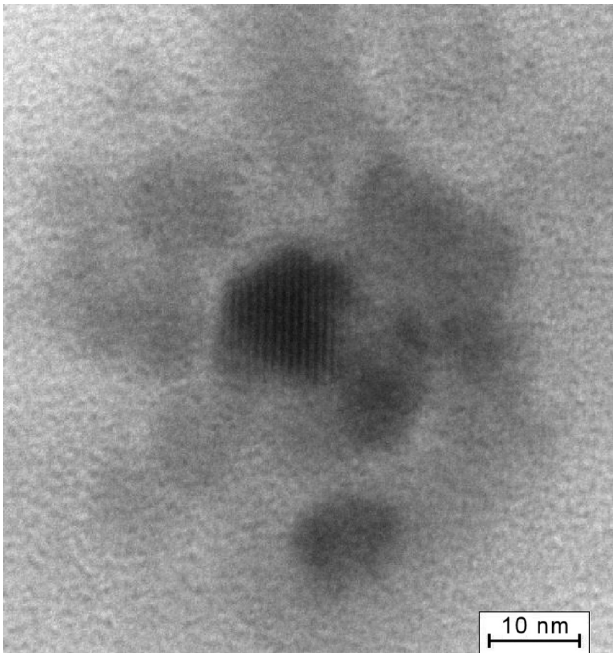

Figure 8. HRTEM image of a single NP showing well-defined lattice fringes.

function of the surface charge of the particles, of the adsorbed layers at the interface, and of the nature and the composition of the surrounding suspension medium. For our Pd colloids, the ζ values are ∼28 mV in the case of low fluence and ∼20 mV at very high fluences. Moreover, in the latter case, the value of ζ potential is unstable, tending to zero during the measurement. In the case of large values of ζ potential, the electrostatic repulsion between particles dominates over the weak attraction due to van der Waals forces, resulting in stable NPs, which explains the higher stability of colloids produced at lower laser fluences. The negative charge present on the surface could be caused by the adsorption of hydroxyl groups OH^- onto the NP surface, as already observed in other colloids produced in aqueous solutions.[3] Alternatively, as suggested by Sylvestre et al.,[35] in the case of gold NPs, the negative charge could be produced by the presence of O^- species on the NP surface, whose formation and abundance is dictated by the PH of the solution. According to Silvestre et al., the O^- species are formed by the hydroxilation of oxide compounds on the NPs surface.

The lower value of ζ-potential obtained at higher fluences could be produced by the presence of Pd^{2+} ions in the solution, as clearly shown from the UV−vis spectra, which reduce the overall charge in the NP solvation sphere. Palladium ions partially and progressively neutralize the negative charge on

dx.doi.org/10.1021/jp109281q |J. Phys. Chem. C 2011, 115, 5073–5083

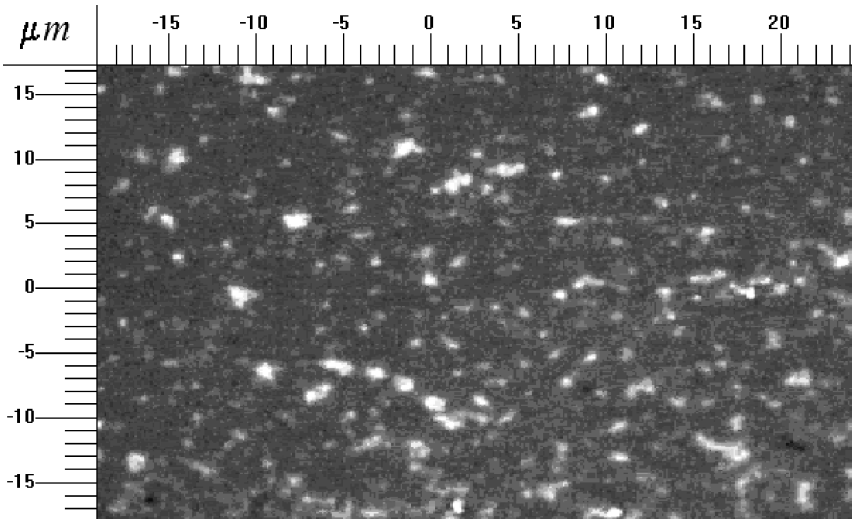

Figure 9. Microscope image of Pd particles deposited on glass.

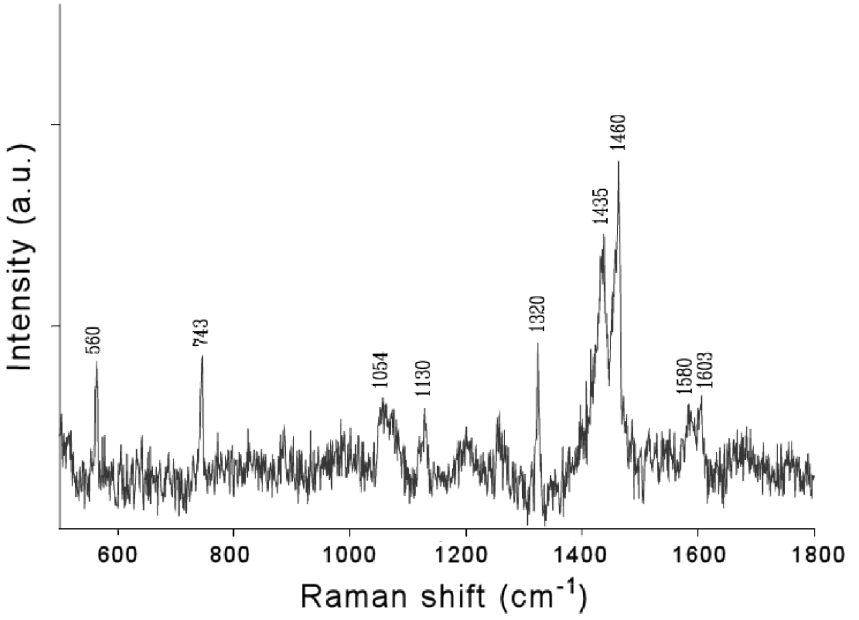

Figure 10. SERS spectrum of phen adsorbed on Pd particles deposited on glass. Excitation: 785-nm laser line.

the NP surface, e.g., producing the desorption of OH^- groups, causing aggregation and precipitation of the metal particles. The large presence of Pd ions in the colloid obtained at large fluences seems confirmed also by the larger measured conductance (~300 μS) with respect to that measured in colloids obtained at low fluences (~141 μS).

(c). SERS Activity. Usually, SERS spectroscopy finds practical applications only for surfaces of coinage metals such as silver, gold, and copper. This occurs because the SERS effect is closely related to the resonance of the laser line used in the Raman excitation with the surface plasmon resonance (SPR) band of the electrons localized at the surface of the metal NPs. For Ag, Au, or Cu NPs, the SPR bands are observed in the visible region (380−800 nm); the resonance peaks of Pd NPs, instead, occur in the UV region, thus impairing the use of laser lines in the visible region for obtaining a reliable SERS effect.[36] This latter, however, was obtained by suitably tailoring the size and the shape of the Pd particles employed in the Raman measurements,[37,38] resulting in a change of their extinction spectrum and, then, in a better coupling with the laser exciting radiation.

In the present study we have checked the adsorption of an organic ligand such as 1,10-phenanthroline (phen) on Pd NPs by Raman measurements. No appreciable SERS signal is observed with the 514.5 nm exciting line in Pd colloids obtained by laser ablation after addition of phen (10^{-4} M). This is closely related to the absence of SPR bands of the Pd NPs in the visible region, as shown in Figure 2. However, a few hours after the addition of phen, the Pd colloidal suspensions become quite unstable, because metal particles aggregate and then collapse. Such evidence suggests that phen molecules are really adsorbed on the palladium surface, by substituting hydroxide or oxygen ions derived from the water environment and allowing the colloidal aggregation, as well as occurring for phen adsorbed on silver colloids.[39] The adsorption of phen is confirmed by

Table 1. Raman Bands (wavenumbers in cm^{-1}) of Phen and Phen/Pd(II) Complex,[13] Compared with the SERS Bands of Phen Adsorbed on Pd Particles

phen	phen/Pd(II) Cl_2	phen/Pd NPs	assignment [a]
552	562	560	δ(phen)
711	743	743	δ(phen)
1035	1050	1054	ν_s(phen)
1136	1139	1130	ρ(C−H)
1345	1310	1320	ν_s(phen)
1405	1427	1435	ν_s(C=C)
1446	1452	1460	ν_s(phen)
1588	1579	1580	ν_{as}(phen)
1601	1601	1603	ν_s(phen)

[a] in-plane modes: ν = stretching, δ = bending, ρ = rocking.[13]

micro-Raman measurements performed on collapsed Pd particles, deposited on glass as a dry layer, by laser excitation at 785 nm. Actually, large Pd aggregates are present, visible with the microscope of the Raman instrument (Figure 9), with dimensions ranging from 500 nm to a few micrometers. With these Pd large particles a sizable SERS effect can be detected, as reported in Figure 10, where the bands appear quite near those observed in the normal Raman spectrum of the Pd(II)(phen)Cl_2 coordination compound,[40] as shown in Table 1.

Moreover, the close similarity between the SERS bands of phen adsorbed on palladium and the Raman bands of the Pd(II) complex indicates that positively charged active sites are really present on the surface of the Pd NPs, which promote the formation of surface complexes with metal\ligand interactions quite similar to coordination bonds.

A further proof that a SERS effect really occurs from our Pd NPs derives from the Raman observation of diluted aqueous solutions of phen deposited on glass, with the same instrument, exciting line, laser power, and focalization conditions of the SERS measurement performed on deposited phen/Pd particles. No Raman signal is detectable with 10^{-4} M concentration of phen, which, instead, gives rise to the SERS spectrum of Figure 10 in the presence of Pd particles.

Finally, it is important to underline that we have performed Raman measurements essentially to verify the capability of Pd NPs to be functionalized with organic molecules. The evaluation of the SERS enhancement factors has not been taken into account, because the determination of the real amount of the adsorbate is not easily achieved.

CONCLUSIONS

Palladium NPs were produced by PLA in aqueous solution, with and without addition of SDS, and successively characterized by UV−vis spectroscopy, TEM-EDS, ζ-potential, and SERS. The process of laser ablation at varying experimental parameters was investigated by estimating the NP mass yield and by the direct imaging of plasma emission. At low laser fluences, the shielding of the laser pulse by the induced plasma is reduced, so that most of the laser energy turns out in mass removal and atomization; however, in that condition, the NP production is limited by the small energy available. On the other hand, at fluences larger than ~12 J cm^{-2}, a plasma forms at the air−water interface and absorbs part of the laser energy via inverse bremsstrahlung processes; this phenomenon becomes stronger with increasing the laser fluence, hence significantly reducing the energy reaching the target and the NP production rate. The optimal conditions for NP production are thus obtained by using an intermediate fluence of ~21 J cm^{-2} and by strongly defocusing the laser beam. The produced NPs are spheroidal, with a polycrystalline structure and an average size in the range 5−15 nm, depending on the experimental conditions. NPs produced at the lower fluences have smaller dimensions with narrow distributions while those obtained at larger fluences have larger dimensions with broader distributions. The addition of SDS results in narrower size distributions, with a strong reduction of larger particles. In a period of 30 days, all the colloids, except those obtained at very high laser fluences, are stable, which probably may be attributed to the presence of OH^- group or O^- species on their surface, that electrostatically prevents particle aggregation. The addition of SDS does not improve NP stability. The colloids produced at very large fluences are unstable, probably because of the presence of Pd ions in the solution, which neutralize the negative charges on the NP surface, causing their aggregation and collapse.

Finally, our Pd particles have an appreciable SERS activity, inferred by the spectroscopic analysis of their aggregates, demonstrating the capability of adsorbing organic molecules. This represents a necessary prerequisite for possible applications of these particles, when functionalized with suitable ligands.

AUTHOR INFORMATION

Corresponding Author

*E-mail: gabriele.cristoforetti@cnr.it; tel.: +390503152222; FAX: +390503152576.

ACKNOWLEDGMENT

The authors gratefully thank the Italian Ministero dell'Università e Ricerca for the financial support and Dr. F. Gambinossi (Dept. of Chemistry, Florence) for his help in ζ potential measurements. This work was supported by MIUR Grants PRIN 2008.

REFERENCES

(1) Taylor, U.; Klein, S.; Petersen, S.; Kues, W.; Barcikowski, S.; Rath, D. *Cytometry, Part A* **2010,** *77A*, 439–446.

(2) Petersen, S.; Barcikowski, S. *J. Phys. Chem. C* **2009,** *113*, 19830–19835.

(3) Mafunè, F.; Kohno, J. Y.; Takeda, Y.; Kondow, T. *J. Phys. Chem. B* **2003,** *107*, 4218–4223.

(4) Park, D. K.; Lee, S. J.; Lee, J. H.; Choi, M. Y.; Han, S. W. *Chem. Phys. Lett.* **2010,** *484*, 254–257.

(5) Kim, S.; Yoo, B. K.; Chun, K.; Kang, W.; Choo, J.; Gong, M. S.; Joo, S. W. *J. Mol. Catal. A* **2005,** *226*, 231–234.

(6) Nishihata, Y.; Mizuki, J.; Akao, T.; Tanaka, H.; Uenishi, M.; Kimura, M.; Okamoto, T.; Hamada, N. *Nature* **2002,** *418*, 164–166.

(7) Thomas, J. M.; Johnson, B. F. G.; Raja, R.; Sankar, G.; Midgley, P. A. *Acc. Chem. Res.* **2003,** *36*, 20–30.

(8) Schlapbach, L.; Züttel, A. *Nature* **2001,** *414*, 353–358.

(9) Manocchi, A. K.; Seifert, S.; Lee, B.; Yi, H. *Langmuir* **2010,** *26*, 7516–7522.

(10) Manocchi, A. K.; Horelik, N. E.; Lee, B.; Yi, H. *Langmuir* **2010,** *26*, 3670–3677.

(11) Wu, S.; Wu, J.; Liu, Y.; Ju, H. *Chem. Mater.* **2008,** *20*, 1397–1403.

(12) Creamer, N. J.; Mikheenko, I. P.; Yong, P.; Deplanche, K.; Sanyahumbi, D.; Wood, J.; Pollmann, K.; Merroun, M.; Selenska-Pobell, S.; Macaskie, L. E. *Catal. Today* **2007**, *128*, 80−87. 0

(13) Hwang, C. B.; Fu, Y. S.; Lu, Y. L.; Jang, S. W.; Chou, P. T.; Wang, C. R. C.; Yu, S. J. *J. Catal.* **2000,** *195*, 336–341.
(14) Le Ru, E. C.; Etchegoin, P. G. *Principles of Surface-Enhanced Raman Spectroscopy and Related Plasmonic Effects*; Elsevier: Amsterdam, 2009.
(15) Wu, B.; Shin, Y. C. *Appl. Phys. Lett.* **2006,** *88*, 041116.
(16) Berthe, L.; Fabbro, R.; Peyre, P.; Tollier, L.; Bartnicki, E. *J. Appl. Phys.* **1997,** *82*, 2826–2832.
(17) Chen, W.; Cai, W.; Lei, Y.; Zhang, L. *Mater. Lett.* **2001,** *50*, 53–56.
(18) Cardenas-Trivino, G.; Segura, R. A.; Reyes-Gasga, J. *Colloid Polym. Sci.* **2004,** *282*, 1206–1212.
(19) Creighton, J. A.; Eadon, D. G. *J. Chem. Soc., Faraday Trans* **1991,** *87*, 3881–3891.
(20) Kumar, C. S. S. R.; Modrow, H.; Hormes, J. *Part. Part. Syst. Charact.* **2002,** *19*, 336–341.
(21) Nichols, W. T.; Sasaki, T.; Koshizaki, N. *J. Appl. Phys.* **2006,** *100*, 114912.
(22) Mafunè, F.; Kohno, J. Y.; Takeda, Y.; Kondow, T.; Sawabe, H. *J. Phys. Chem. B* **2000,** *104*, 8333–8337.
(23) Kreibig, U.; Vollmer, M. *Optical Properties of Metal Clusters*; Springer: Berlin, 1995.
(24) Nichols, W. T.; Sasaki, T.; Koshizaki, N. *J. Appl. Phys.* **2006,** *100*, 114913.
(25) Vogel, A.; Noack, J.; Nahen, K.; Theisen, D.; Busch, S.; Parlitz, U.; Hammer, D. X.; Noojin, G. D.; Rockwell, B. A.; Birngrube, R. *Appl. Phys. B: Laser Opt.* **1999,** *68*, 271–280.
(26) Cristoforetti, G.; Legnaioli, S.; Palleschi, V.; Tognoni, E.; Benedetti, P. A. *J. Anal. Atom. Spectr* **2008,** *23*, 1518–1528.
(27) Golightly, J. S.; Castleman, A. W. *J. Phys. Chem. B* **2006,** *110*, 19979–19984.
(28) Mafunè, F.; Kohno, J. Y.; Takeda, Y.; Kondow, T.; Sawabe, H. *J. Phys. Chem. B* **2000,** *104*, 9111–9117.
(29) Granqvist, C. G.; Buhrman, R. A. *J. Appl. Phys.* **1976,** *47*, 2200–2219.
(30) Kabashin, A. V.; Meunier, M. *J. Appl. Phys.* **2003,** *94*, 7941–7943.
(31) Bozon-Verduraz, F.; Brayner, R.; Voronov, V. V.; Kirichenko, N. A.; Simakin, A. V.; Shafeev, G. A. *Quant. Electron* **2003,** *33*, 714–720.
(32) Simakin, A. V.; Voronov, V. V.; Kirichenko, N. A.; Shafeev, G. A. *Appl. Phys. A: Mater. Sci. Process.* **2004,** *79*, 1127–1132.
(33) Mafune, F.; Kohno, J. Y.; Takeda, Y.; Kondow, T.; Sawabe, H. *J. Phys. Chem. B* **2001,** *105*, 5114–5120.
(34) Wen, S. B.; Mao, X.; Greif, R.; Russo, R. E. *J. Appl. Phys.* **2007,** *101*, 123105.
(35) Sylvestre, J. P.; Poulin, S.; Kabashin, A. V.; Sacher, E.; Meunier, M.; Luong, J. H. T. *J. Phys. Chem. B* **2004,** *108*, 16864–16869.
(36) Cui, L.; Wang, A.; Wu, D. Y.; Ren, B.; Tian, Z. Q. *J. Phys. Chem. C* **2008,** *112*, 17618–17624.
(37) Xiong, Y.; McLellan, J. M.; Chen, J.; Yin, Y.; Li, Z. Y.; Xia, Y. *J. Am. Chem. Soc.* **2005,** *127*, 17118–17127.
(38) Liu, Y.; Hu, J.; Kong, Q.; Feng, X. *Mater. Lett.* **2010,** *64*, 422–424.
(39) Muniz-Miranda, M.; Pergolese, B.; Bigotto, A.; Giusti, A. *J. Colloid Interface Sci.* **2007,** *314*, 540–544.
(40) Makedonas, C.; Mitsopoulou, C. A. *Spectrochim. Acta A* **2006,** *64*, 918–930.